SANDIA REPORT

SAND95-0086 • UC-904
Unlimited Release
Printed April 1997

Computer Simulation of Solder Joint Failure

S. N. Burchett, D. R. Frear, M. M. Rashid

Prepared by
Sandia National Laboratories
Albuquerque, New Mexico 87185 and Livermore, California 94550

Sandia is a multiprogram laboratory operated by Sandia Corporation, a Lockheed Martin Company, for the United States Department of Energy under Contract DE-AC04-94AL85000.

Approved for public release; distribution is unlimited.

Sandia National Laboratories

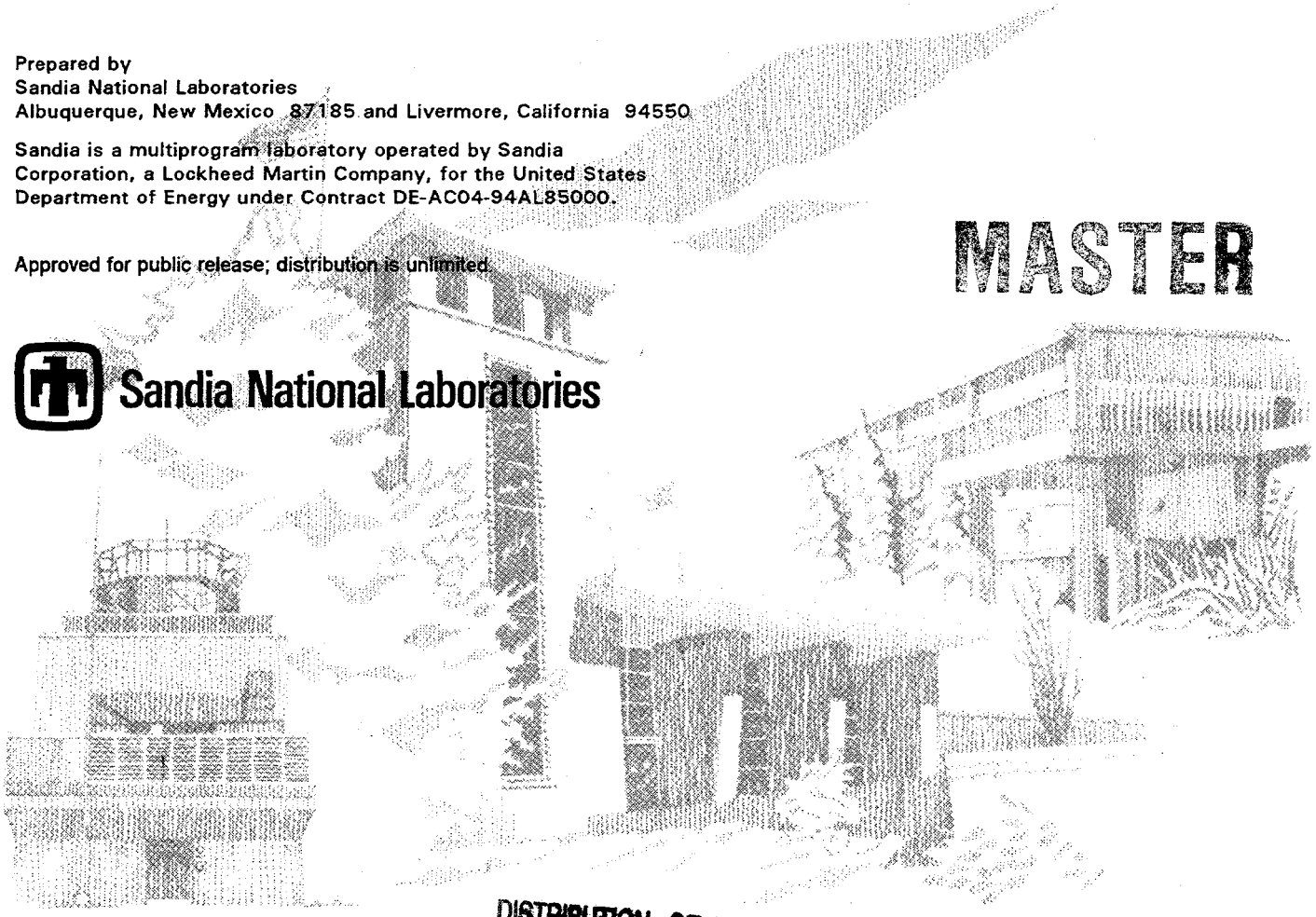

SF2900Q(8-81)

Issued by Sandia National Laboratories, operated for the United States Department of Energy by Sandia Corporation.

Available to DOE and DOE contractors from
Office of Scientific and Technical Information
P.O. Box 62
Oak Ridge, TN 37831

Prices available from (615) 576-8401, FTS 626-8401

Available to the public from
National Technical Information Service
U.S. Department of Commerce
5285 Port Royal Rd
Springfield, VA 22161

NTIS price codes
Printed copy: A03
Microfiche copy: A01

SAND95-0086
Unlimited Release
Printed April 1997

Distribution
Category UC-904

Computer Simulation of Solder Joint Failure

S. N. Burchett
Engineering Mechanics and Materials Modeling Department
D. R. Frear
Mechanical and Corrosion Metallurgy Department
Sandia National Laboratories
P.O. Box 5800-0443
Albuquerque, NM 87185-0443
and
M. M. Rashid
University of California, Davis
Davis, CA

Abstract

The thermomechanical fatigue failure of solder joints is increasingly becoming an important reliability issue for electronic packages. The purpose of this Laboratory Directed Research and Development (LDRD) project was to develop computational tools for simulating the behavior of solder joints under strain and temperature cycling, taking into account the microstructural heterogeneities that exist in as-solidified near eutectic Sn-Pb joints, as well as subsequent microstructural evolution. We present two computational constitutive models, a two-phase model and a single-phase model, that were developed to predict the behavior of near eutectic Sn-Pb solder joints under fatigue conditions. Unique metallurgical tests provide the fundamental input for the constitutive relations. The two-phase model mathematically predicts the heterogeneous coarsening behavior of near eutectic Sn-Pb solder. The finite element simulations with this model agree qualitatively with experimental thermomechanical fatigue tests. The simulations show that the presence of an initial heterogeneity in the solder microstructure could significantly degrade the fatigue lifetime. The single-phase model was developed to predict solder joint behavior using materials data for constitutive relation constants that could be determined through straightforward metallurgical experiments. Special thermomechanical fatigue tests were developed to give fundamental materials input to the models, and an *in situ* SEM thermomechanical fatigue test system was developed to characterize microstructural evolution and the mechanical behavior of solder joints during the test. A shear/torsion test sample was developed to impose strain in two different orientations. Materials constants were derived from these tests. The simulation results from the two-phase model showed good fit to the experimental test results. The single-phase model could be very useful for conditions where microstructural evolution is not a dominant factor in fatigue, but has limitations in attempting to predict the behavior of near eutectic Sn-Pb solders. The models show a great deal of promise for capturing the fundamental behavior of solder that is needed to predict reliability. However, using these complex models requires mechanics and materials expertise and computing resources beyond that generally available to designers of electronic packages. Therefore, a natural continuation of this project would be to develop a format that is immediately useful for designers in creating electronic systems with interconnections that have a known high degree of reliability.

Acknowledgments

The support of Sandia National Laboratories LDRD office is acknowledged. The authors would like to acknowledge the experimental assistance of J. L. Finch and T. Rice for their work on the thermomechanical fatigue tests and S. Brandon for his work on the shear/torsion tests. The review of the manuscript by Mike Hosking and Mike Neilsen is also greatly appreciated.

Table of Contents

Introduction

Solder joints were initially designed to be simple electrical interconnections between mechanically interlocked components in electronic packages. As technology advanced, electrical component size decreased, and the number of input/output terminations increased. To accommodate these changes, the numbers of solder joints per package have increased, while joint dimensions have decreased. The mechanically interlocked components were replaced by plated-through-hole technology, which is now being replaced by surface mount technology (SMT). With each technological advance, the solder joint was expected to be not only an electrical conductor, but also an increasingly important structural member, with a smaller and smaller feature (solder joint) size. The benefits of shrinking solder joint dimensions are numerous (e.g., increased speed, greater packing density, etc.), but the reliability concerns increase with decreasing dimensions.

Furthermore, the reliability of solder joints under conditions of thermomechanical fatigue becomes more critical as new electronic packaging technologies evolve. In the future, larger silicon devices and the rapidly evolving multi-chip module will cause larger strains to be induced in the joints. The service environment of the solder joints is also becoming more severe. New power devices are running hotter. For example, electronic packages are positioned closer to the engine in automobiles for faster response and greater cost effectiveness. For increased automobile fuel efficiency, styling is more streamlined and air inlets are decreasing. This results in higher operating temperatures under the hood and greater strains in the solder joints. In avionic applications, electronic packages used for sensing, control and telemetry are exposed to severe ambient environmental temperature swings. The severity and frequency of these environmental cycles creates large cyclical strains in the solder joints. Therefore, a means of determining the reliability of solder joints is critical for improving the quality of an electronic system.

A key issue in the long term reliability of solder joints is joint failure during thermal cycling. The individual components that are soldered together in an electronic package typically have differing thermal expansion coefficients. For example, an SMT ceramic chip carrier with a coefficient of thermal expansion of approximately $6 \times 10^{-6}/^{\circ}C$ is soldered to a polyamide circuit board with a thermal expansion of approximately $15 \times 10^{-6}/^{\circ}C$. When the soldered assembly encounters thermal fluctuations (due to internal heating or changes in ambient temperature) strain is imparted to the joint. Nominally, the imposed strains can range from less than 1% to as high as 20%. These thermally induced cyclic strains result in thermomechanical fatigue and often failure of the solder joints. Thermally induced cyclic strain is the primary cause of reliability in solder interconnections.

In the past, strain was minimized in solder joints by designing leads with "stress loops" to isolate deformation from the solder. Strain to the solder joints is alleviated by the compliant leads that are attached to components. This method of strain relief reduces the amount of damage to the joint. One problem with this solution is that the higher profile and space requirements of the package prevents miniaturization. That is, the increased package size cannot provide the greater density and speed of modern technologies such as SMT. With SMT, the majority of the thermal expansion mismatch strain is taken up entirely by the solder. Initially, this was thought to be good since the solder was "compliant" and would take up the strain without damage. However, there is still enough cyclic damage to cause fatigue failures (Pan and Winterbottom 1990, and Lau and Harkins 1988). An

example of a solder joint fatigue failure in a surface mount solder joint is shown in Figure 1.

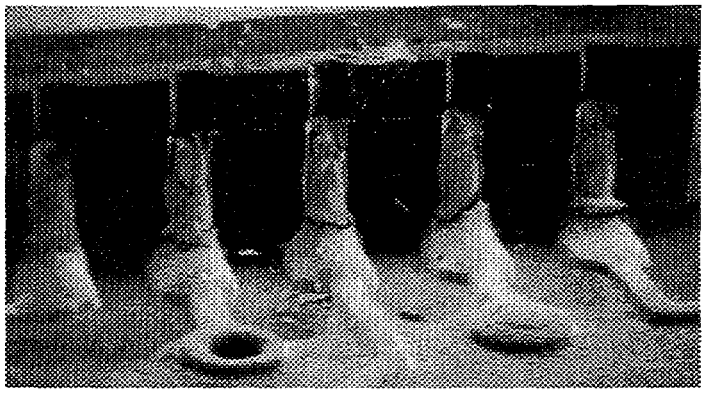

Figure 1 SEM micrograph of surface mount solder joints that failed under conditions of thermomechanical fatigue.

The alloy most commonly used as an interconnect in electronic packaging is near eutectic 60Sn-40Pb (wt.%) solder. This alloy is used because its low melting temperature of 183°C makes the solder processing compatible with the other materials used in a package. The 60Sn-40Pb alloy also has good wetting behavior and bonds well to the copper metallizations typically used in electronics assembly. The low melting temperature is a benefit from the point of view of producibility but could detrimentally influence lifetime reliability. At room temperature, 60Sn-40Pb is at 0.6 of its absolute melting temperature or homologous temperature, T_h. In severe avionics applications, the temperature cycle of -55°C to 125°C is between $0.4T_h$ and $0.9T_h$. Due to the high homologous temperatures experienced by solder alloys under these service conditions, the solder may exhibit such phenomena as viscoplasticity (i.e., creep), grain growth, hardening and/or softening due to dislocation substructure evolution, and grain boundary sliding and separation. Further, as-cast solder joints typically exhibit macro-scale heterogeneities in the arrangement of their microstructural features. Figure 2 is an optical micrograph of an as-solidified 60Sn-40Pb solder joint that shows these microstructural features. Since 60Sn-40Pb is on the Pb-rich side of the eutectic, proeutectic Pb dendrites are present. Dendrite formation occurs during the initial stages of solidification. The eutectic structure in the joint consists of lamellar and globular regions of Pb-rich and Sn-rich phases. The regions of similarly oriented lamella are separated into individual cells, or colonies. These colonies develop during solidification of the eutectic from a variety of nuclei on the solid base metal surface. The solidifying lamella grow into the molten solder and eventually intersect with other solidifying cells. The regions where the cells intersect are coarsened with respect to the lamellar structure inside the colony, and are the last regions of the joint to solidify. The initial inhomogeneous microstructure of the solder joint, combined with the cyclical high homologous temperatures and deformation mechanisms, can cause the microstructure of the joint to dramatically change.

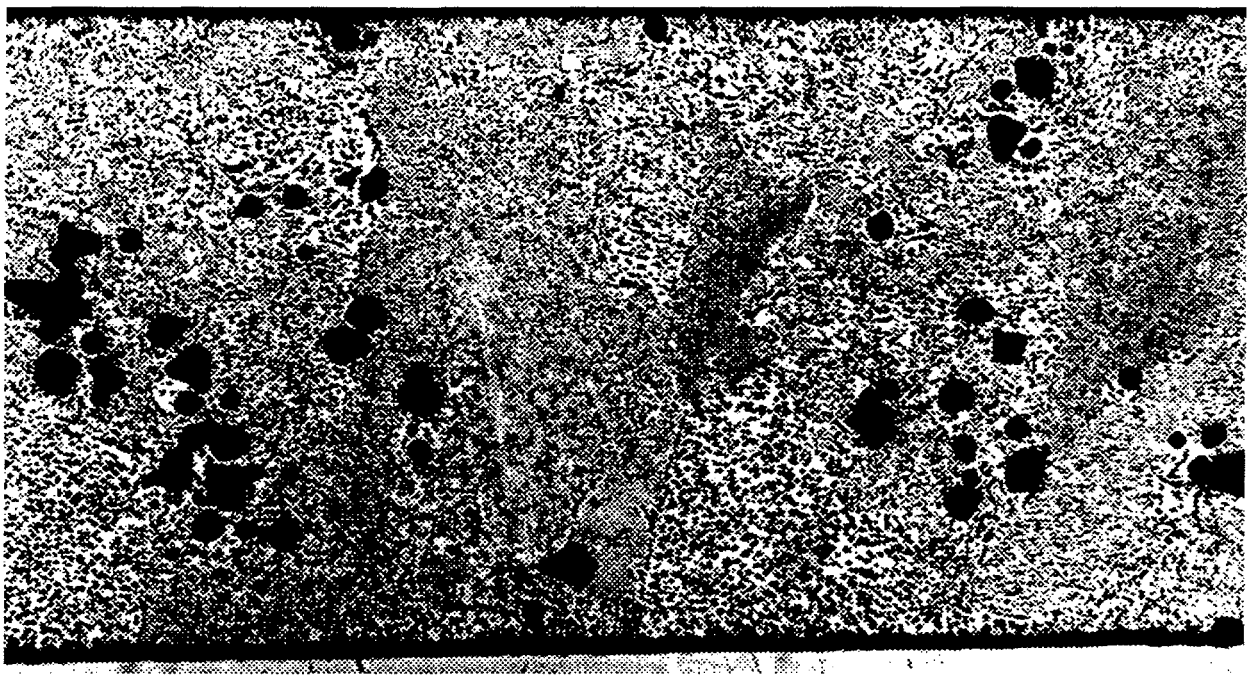

Figure 2 Microstructure of the as-solidified 60Sn-40Pb solder joint. The dark regions are the Pb-rich phase the light regions are the Sn-rich phase.

Since the structure of the 60Sn-40Pb alloy is not homogeneous or isotropic, it deforms heterogeneously under thermomechanical fatigue conditions. The series of optical micrographs in Figure 3 shows the evolution of the solder microstructure during 10% shear strain cycling for a thermal cycle of -55° to 125°C. The deformation concentrates at cell boundaries in the microstructure resulting in additional coarsening. Eventually, cracks form in these coarsened regions resulting in mechanical and electrical failure. In order to ensure the reliability of a given electronic system, a thermomechanical fatigue life prediction methodology is needed

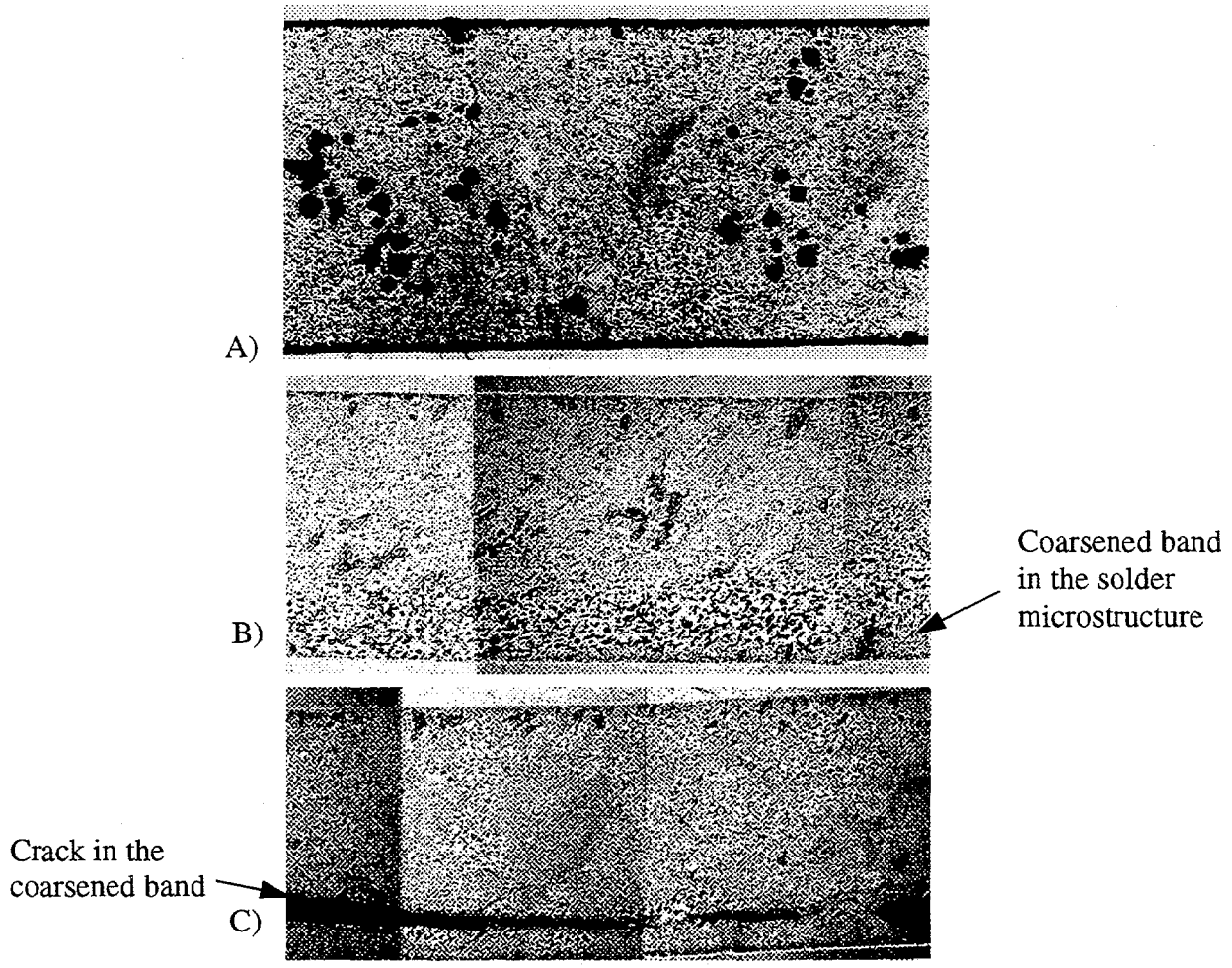

Figure 2 Heterogeneous coarsening in 60Sn-40Pb solder joints. A) As solidified, B) Heterogeneous Coarsening, C) Failure through the coarsened band.

A number of methodologies have been proposed for determining reliability through lifetime prediction of solder joints under conditions of thermomechanical fatigue. A detailed summary and critical review of these methodologies is found elsewhere (Sandor 1991 and Solomon 1993). However, it is appropriate to discuss the salient points of current methodologies. A common shortfall of these methodologies is that they are empirical in nature and do not include the microstructural evolution that occurs in 60Sn-40Pb solder during thermomechanical fatigue.

Current Lifetime Prediction Methodologies

The damage mechanism to solder joints in electronic assemblies is strain-based low cycle fatigue. The most common technique to determine the lifetime of solder joints is based on the Coffin-Manson low cycle fatigue relationship [Coffin 1954, Manson 1953, Manson 1960 and Coffin 1969], which relates fatigue life, N_f, to the change in elastic and inelastic strain per load cycle:

$$\Delta\gamma = \frac{\sigma_f'}{E}(2N_f)^b + \varepsilon_f'(2N_f)^c \qquad \text{Eqn. (1)}$$

where b and c are constants (and are derived from experimental data), σ_f' and ε_f' are the fatigue ductility coefficients (that are also empirically derived from experimental fatigue tests), and E is the elastic modulus.This methodology was developed for pressure vessel steels (AISI 304 stainless steel in particular) that underwent cyclic loading [Majumdar and Jones 1991]. For solder joints, the elastic portion of the equation $\left(\frac{\sigma_f'}{E}(2N_f)^b\right)$ is negligible and the fatigue life can be estimated as:

$$N_f = \frac{1}{2}\left(\frac{\Delta\gamma}{\varepsilon_f'}\right)^{\frac{1}{c}} \qquad \text{Eqn. (2)}$$

Life is estimated using low cycle isothermal fatigue experiments at a variety of strain ranges, drawing a straight line on a log-log plot of N_f *versus* $\Delta\gamma$ and extrapolating these values to the desired strain range. The shortcoming of this methodology is that it is based solely upon the curve fitting of experimentally derived data (normally isothermal fatigue tests). The values of c and ε_f' are empirical and are not fundamental by any means. Therefore, life prediction can be made only after accelerated testing of a large number of solder joints with the assumption (not always valid) that the accelerated test results mirror real use conditions.

The Coffin-Manson formulation presented above is also inadequate when there is a great deal of time-dependent deformation (as occurs in solder joints) [Coffin 1971]. This inadequacy has been addressed by accounting for frequency effects in the equation. This modified formulation is written as:

$$N_f = \frac{1}{2}\left(\frac{\Delta\gamma}{\varepsilon_f'\upsilon^{k-1}}\right)^{\frac{1}{c}} \qquad \text{Eqn. (3)}$$

where ν is the cycling frequency and k is an empirical material parameter.The value of k is determined by fitting the equation to the data. Again, like the modified Coffin-Manson formulation, the basis for life prediction is empirical curve fitting of existing data. Another severe limitation of this method is that the formulation works only for sinusoidal strain cycles. The formulation was derived from laboratory work where sinusoidal waveshapes are easy to generate. However, the service loads with solder are generally not sinusoidal. Furthermore, the life plots associated with the frequency modified formulation often have a bilinear appearance. These complexities are likely due to several factors, including microstructural instability. No Coffin-Manson based formulation can treat this behavior explicitly.

To use these methods, one must know, or compute, the shear strain, γ. Nevertheless, a great deal of recent solder lifetime prediction modeling has been based on the Coffin-Manson relation. This effort has focused on determination of the strains (and stresses) in the solder joint by using improved finite element models. Once the strains are determined, the lifetime is predicted by com-

paring the computed strains to an experimentally derived Coffin-Manson plot of strain versus the number of cycles to failure. Examples of these efforts include the following. Lau and Erasmus (1993) studied 304 pin Quad-Flat-Pack joints with constitutive assumptions that the solder is elastic-fully plastic. Sauber and Seyyedi (1992), used a power law creep model in a finite element simulation to calculate the solder joint creep response on leaded devices. Ross, et al. (1992) also modeled leaded devices and included both creep and creep ratcheting in the algorithm to determine stresses and strains in the solder joints. Schmidt (1992) developed a life prediction model of leadless solder joints using incremental damage summation to predict life.

A phenomenological model for solder joint life prediction has been proposed by a variety of workers (Verma, et al., 1993; Dasgupta, et al., 1992; Huang, et al., 1994) that is based on energy partitioning. In this methodology, the elastic, plastic, and creep energy components of strain energy are computed from an empirical fit of experimental hysteresis loops.The life is predicted using an incremental damage accumulation model.

Strain Range Partitioning (Solomon, 1994) is another modification of the Coffin-Manson formulation where an interactive cumulative damage rule is used to determine the fatigue life when there are combinations of plasticity and creep:

$$\frac{1}{N_f} = \frac{F_{pp}}{N_{pp}} + \frac{F_{cc}}{N_{cc}} + \frac{F_{cp}}{N_{cp}} + \frac{F_{pc}}{N_{pc}} \qquad \text{Eqn. (4)}$$

where N_f is the fatigue life, F_{pp} is the fraction of the deformation which is no creep or tension in compression (PP), N_{pp} is the fatigue life when pure PP deformation is used, and F_{cc}, N_{cc}, etc., correspond to CC (creep deformation in both tension and compression), CP (creep in tension but no creep in compression) and PC (no creep in tension but creep in compression) deformations. The fraction of life is determined by analyzing load *versus* strain hysteresis loops generated in isothermal fatigue tests. The difficulties in using strain range partitioning for solders are many. First, the technique does not take into account material property changes due to microstructural evolution. The SRP method also requires extensive data for determining N_{ij} and F_{ij}. Furthermore, it is extremely difficult to measure the required inelastic strain components accurately in real solder joints. Finally, there is a great lack of SRP data for the shear mode of deformation, and some doubts exist as to whether the technique is even applicable in shear.

Note that the Coffin-Manson based formulations described above do not take solder alloy, processing history, or microstructure into account. The Coffin-Manson formulation assumes that the material is monolithic and is time/history independent.

Fracture Mechanics lifetime approaches, [Lau 1993, Pao et al. 1993, Pao and Pan 1990, Wong et al. 1988, Yamada 1988 and 1989], have also been applied to solder joints most notably the J and C* approaches [Solomon et al. 1990]. The fracture mechanics approach assumes failure occurs when a crack, that initiates on the first cycle, propagates through the joint. Pao and coworkers [1993] developed a constitutive relation based on creep and elastic deformation to model the behavior of 90Pb-10Sn solder joints and used the fracture mechanics relation of crack driving force, C*, to model failure. They found fracture mechanics works well for large strains but underestimates life at small strains. Lau proposed to use fracture mechanics to predict the thermal fatigue life of solders using the stress intensity factor, ΔK, and the Paris law to estimate the crack growth rate in solder. Lau states that this use of fracture mechanics still requires a great deal of develop-

ment due to the extensive assumptions needed to determine life. The most serious limitation to the fracture mechanics approach is that the ductility of the solder necessitates the use of a fairly large testing specimen that may not have a structure or geometry similar to that found in the small solder joints in electronic assemblies. A further limitation is that the microstructure cannot be implicitly included in the model.

The above life prediction techniques treat the solder as a homogeneous continuum and neglect the potentially large effects that the microstructure and heterogeneous deformation have on joint lifetime. A few models have been proposed recently to incorporate the microstructure in some form into the model. The constitutive relations developed by Akay, et al., (1993), Pan and Winterbottom (1990), Hacke, et al., (1993) and Busso, et al., (1994) incorporate materials constants purported to have the form of a grain or phase size. These constitutive relations are then used in a finite element code to predict stress and strain in the joints. Life is then predicted using an empirical Coffin-Manson relation. The effects of heterogeneities in the solder microstructure are discussed in the work of Guo, et al., (1992) who used a dislocation "pile-up" model as part of an effort to predict the deformation hysteresis loops in solder. The effect of the microstructure is incorporated indirectly because the dislocation pile-ups occur at phase and grain boundaries. Sandstrom, et al., (1993) also modeled the isothermal fatigue hysteresis loops of solder that used variations in the dislocation density to incorporate the inhomogeneous microstructure. The solder joint lifetime is again predicted using a Coffin-Manson relation. The microstructure in the above models is static (does not evolve with time) and there is no mechanism to include heterogeneities.

A reliability tool based on Figures of Merit has been developed to estimate fatigue life of solder joints [Clech et al. 1989]. In the Figures of Merit approach, experimental data (such as isothermal fatigue lifetimes and lead compliances) are combined to compare one joint design with another using a series of formulas. This technique is accurate when there is sufficient field data to incorporate into the model. The technique is especially useful for considering small variations in design when the thermal environment is not severe. The methodology breaks down in severe thermal/mechanical environments and for designs where no empirical data exists.

The consistent problem with the currently available solder joint lifetime prediction methodologies is that they are empirically based and therefore specific to the conditions of the test. The models use isothermal fatigue tests where real electronic assemblies undergo thermomechanical fatigue. The solder alloy, its processing history, and microstructure are typically ignored, and the joint is treated as an isotropic, unchanging, homogeneous material. The models are only directly applicable to systems that see the same conditions as the empirically derived data.The empirical data cannot be generally applied. A reliability model that incorporates microstructure, heterogeneities, and microstructural evolution is needed to determine the lifetime of Sn-Pb solder joints under conditions of thermomechanical fatigue.

In this respect, we present a new approach that integrates experimental results and computational techniques to predict fatigue life. It involves the use simplified experimental tests as fundamental input for two constitutive models that can be used in finite element simulations to predict the behavior of the solder joints under deformation conditions. The important aspect of these models is that they incorporate microstructure heterogeneities and microstructural evolution.

Purpose of the LDRD

This Laboratory Directed Research and Development (LDRD) project was undertaken with the goal of developing a computational simulation capability for predicting the long term reliability

behavior of solder joints. Solder joint behavior is complicated by the heterogeneous coarsening of its microstructure coarsens heterogeneously during strain-temperature cycling, leading to strain localization and accelerated coarsening. A joint computational/experimental study was performed in which finite element simulations of solder joints, up to the point at which significant strain localization occurs, were made. The core of the research focussed on developing the constitutive models, especially the test procedures, and validating the simulations against realistic experiments. This research will potentially lay the foundation for future projects involving simulation of a wide variety of microstructural phenomena. It is becoming increasing important that this approach be developed into a reliable paradigm, as performance demands on engineered materials grow ever greater.

Experimental Techniques

In the process of developing solder joint lifetime prediction models a number of experimental and computational techniques were developed. The following is a summary of the metallurgical experiments and techniques. The results of these tests were used as input to the constitutive models discussed later. The solder alloy used in these tests is near eutectic 60Sn-40Pb joined to copper substrates.

Metallurgical Experiments

Thermomechanical Fatigue Tests

The thermomechanical fatigue tests have been performed in a simple shear orientation and provide results on microstructural evolution and solder joint lifetime. This procedure is also described elsewhere (Frear 1989, Frear, et al., 1993). A detailed summary of the test method is given below.

The specimen used to test solder joints is shown in the schematic drawing in Figure 4, and a photo of the assembled specimen is shown in Figure 5. The specimen consists of 18 electrically isolated solder joints that, when the specimen is gripped and pushed and pulled on the ends, deform in shear. The joints are formed by pre-tinning both sides of the pads to be joined with a thin layer of 60Sn-40Pb solder. A pre-measured volume of solder wire is then placed on the center pad as a preform along with a thin coating of a rosin, mildely activated (RMA) flux. The three pieces of the sample are then clamped together using a fixture that creates a 0.010" spacing for the joints. The joints are formed during a reflow step in a tube furnace set at 240°C for 4 minutes. The resultant joints have a simple truncated spherical geometry.

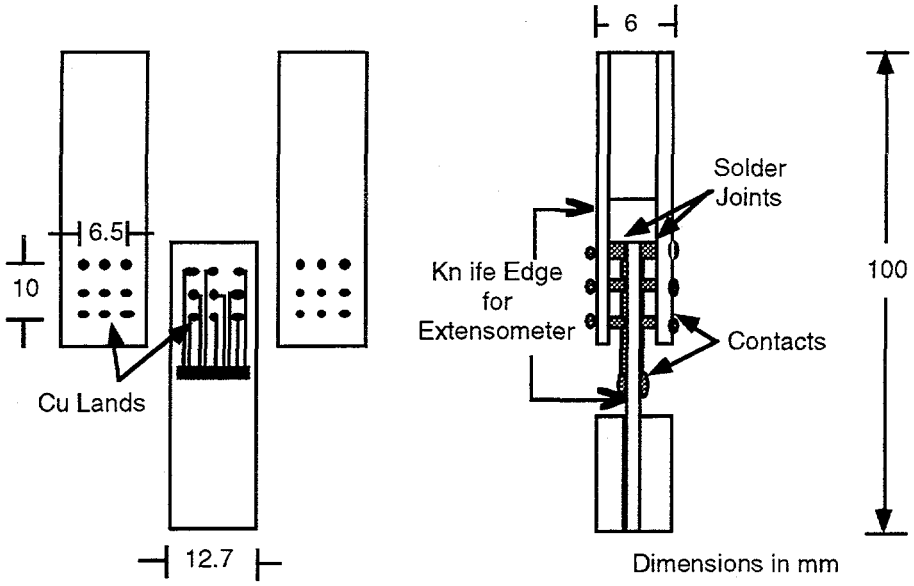

Figure 4 Thermomechanical fatigue test sample.

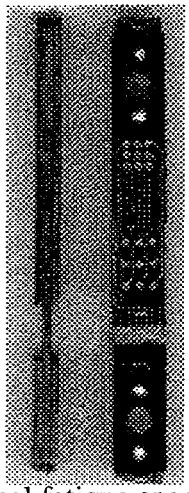

Figure 5 Photograph of the thermomechanical fatigue specimen shown schematically in Figure 4.

Strain is imposed upon the solder joints in the sample by a servohydraulic load frame operated under strain control. Thermal fluctuations are induced by a chamber that fits around the specimen in the load frame. Compressed air is heated and cooled by a commercial heating and cooling system (an FTS Turbojet system) and circulates around the specimen. The strain and temperature are computer controlled. The temperature extremes tested were –55° to 125°C. The total strain imposed was 10% from one end of the cycle to the other. The thermal cycle consists of a ramp in strain and temperature to 125°C followed by a 3 minute hold period, a ramp down to -55°C, followed by another 3 minute hold at -55°C. The deformation rate used for these tests was $2.1 \times 10^{-4} s^{-1}$. Failures were monitored electrically by monitoring spikes in resistance. The electrical data along with load, temperature, and strain were collected and stored on a computer. Tests were run up to 350 cycles

with failures occurring at about 250 cycles. For this study a total of 10 tests were run.

To examine the microstructure of the solder joints after testing, the samples were mounted and metallographically sectioned and polished to reveal the solder microstructure for coarsening and crack formation.

In Situ SEM Thermomechanical Fatigue Tests

Since solders in electronic systems are used at a high fraction of their homologous temperature, the microstructure is expected to evolve during the test. To date, the microstructural characterization methods involve sectioning samples for observation after a given number of cycles. This is a time consuming process and results in only a snapshot of the evolution of the microstructure for each sample. In order to develop a good model, the microstructure must be quantified throughout the deformation process. This can be performed using an *in situ* scanning electron microscope (SEM) equipped with a deformation stage capable of thermal cycling and subsequent image analysis.

In order to examine real time microstructural evolution of solder during fatigue an *in situ* SEM with a deformation stage was built. A schematic illustration of the system is shown in Figure 6 and a photograph of the system and chamber is shown in Figure 7. The SEM is equipped with a servo-hydraulic loadframe (inside the vacuum chamber) that can impose strain on a sample at a constant strain rate while the SEM is collecting images. The specimen for the *in situ* SEM thermomechanical fatigue test is shown in Figure 8. The sample consists of two copper parts that are soldered together with 60Sn-40Pb. The exposed joint is then polished to a smooth surface to reveal the solder microstructure. In order to perform thermomechanical tests on the solder, cyclically heated and cooled air is circulated through a closed loop in the chamber to heat and cool the grips, and therefore the sample. The system is capable of thermally cycling the sample from -25° to 125°C. The deformation is imparted at a rate of 2.1×10^{-4} s^{-1} over a shear strain range of 10%. The operating conditions of the *in situ* SEM were designed to be as similar as possible to the thermomechanical fatigue test described above. The net result is a real time observation of the thermomechanical deformation process of the solder microstructure.

The SEM can be operated in secondary or backscatter mode. For Pb-Sn solder, the difference in atomic weight is great so operating in backscatter mode clearly reveals the structure of the solder. The SEM is a digital storage microscope so that undistorted images can be taken of the solder microstructure during deformation.

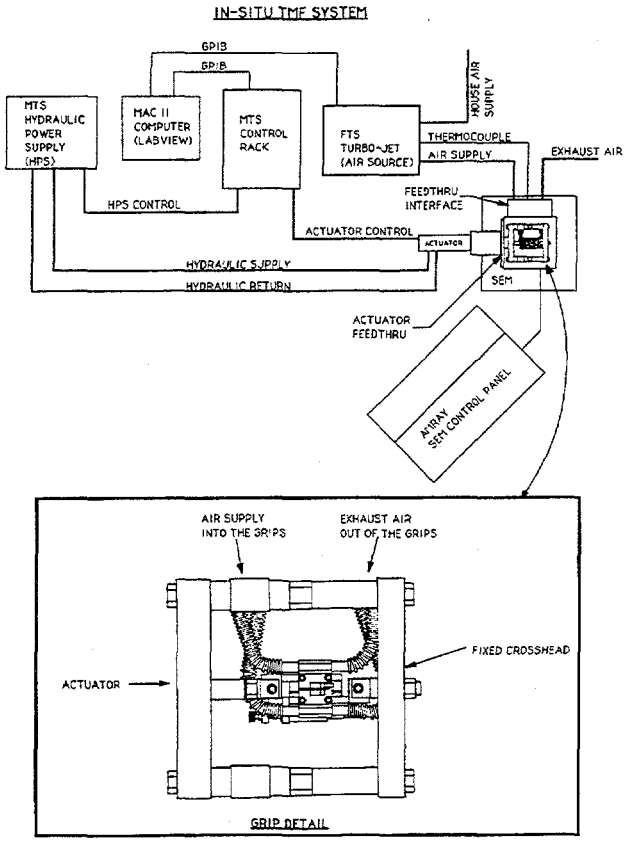

Figure 6 Schematic drawing of the *in situ* SEM used to perform thermomechanical fatigue tests.

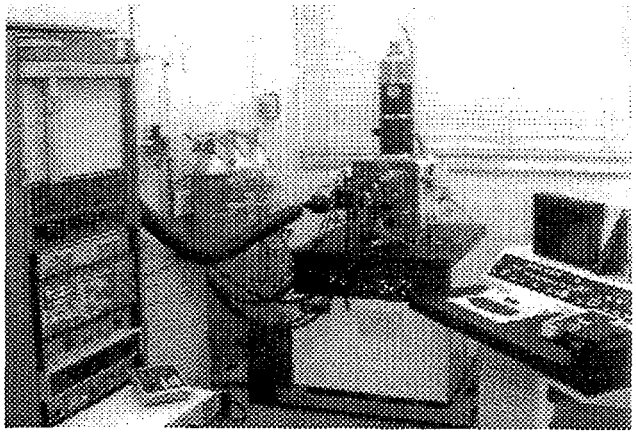

Figure 7 Photograph of the *in situ* SEM system.

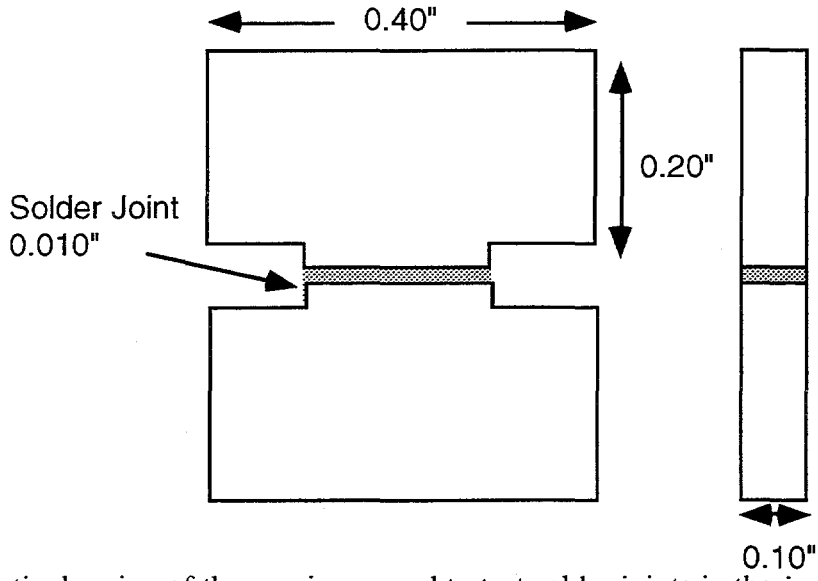

Figure 8 Schematic drawing of the specimen used to test solder joints in the *in situ* SEM thermomechanical fatigue test frame

The microstructural development was quantified by digitizing the analog images from the SEM and capturing them on a hard disk for computer analysis. Any heterogeneities in strain concentrations or the microstructure were then be measured. The digitized microstructure can then be used to compare with the results of the modeling effort.

The results of the *in situ* deformation studies also provided the basis for the determination of microstructural state variables needed for the finite element simulations. The resultant microstructures can be assigned mechanical properties based upon a number of measurable variables (cell size, grain size, phase size and lamellar spacing).

Shear/Torsion Testing of Solder Joints

Constitutive relation information for the single phase constitutive model was in part determined using a specially designed shear/torsion solder joint specimen shown schematically in Figure 9. The test sample has a "ring in plug" design, where pulling along the z-axis results in shear deformation, and axial rotation causes shear deformation in an orientation 90° away from the z-axis. Deforming the sample in these two directions subjects the sample to shear deformation in orthogonal directions. The results of the orthogonal shear deformation were used to determine the material constants for the single-phase constitutive model. The samples were tested in a servo-hydraulic test frame equipped with an electric rotational drive for torsion testing. A total of 5 tests were performed at room temperature with the deformation cycle shown in Table 1

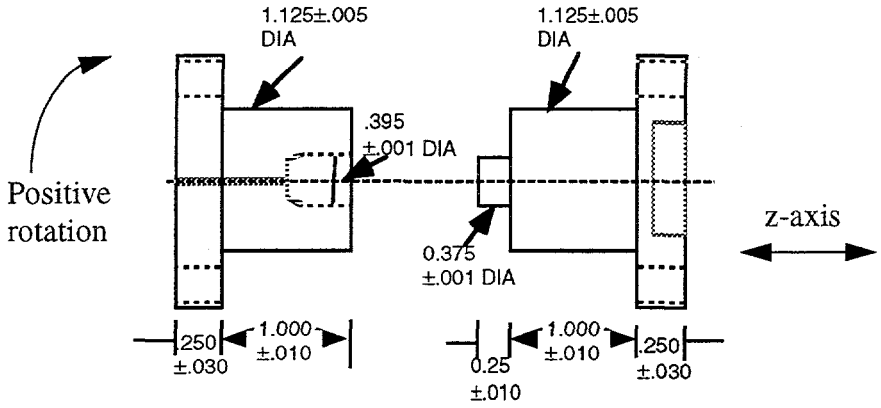

Figure 9 Shear/torsion test sample designed to impose two different orientations of shear strain onto a thin (0.254mm) solder joint. All dimensions are in mm.

Table 1: Shear/Torsion Test

Rotation Rate (deg./sec.)	Deformation Rate (mm/sec.)	Time (seconds)
$3x10^{-4}$	0	600
0	$3.6x10^{-5}$	600
0	0	600
0	$-3.6x10^{-5}$	600
$-3x10^{-4}$	0	600
0	0	600

The conditions in Table I result in an imposed strain rate of $1.0x10^{-4}sec^{-1}$ for the test outside of the stress relaxation regimes. The hold times were included to account for any time dependent deformation that occurs during the deformation cycle. A total of six cycles were imposed on each specimen and a total 8.48% shear strain amplitude. The data, in the form of applied strain versus load, was collected digitally and plotted as load as a function of time.

Constitutive Models

The two-phase and single phase constitutive models have been formulated to describe the thermomechanical response of the 60Sn-40Pb solder alloy. The philosophy and intent underlying each of the two models is different: the two-phase model is intended to be used as a research tool to evaluate the relative importance of certain microstructural phenomena. Microstructural evolution and mechanical behavior inputs to this model are derived from experimental thermomechanical fatigue tests on solder joints. On the other hand, the single-phase model is intended to render meaningful

engineering predictions of stress and strain when used in a finite element code. In this simpler model, the emphasis is on striking a balance between representing complex microstructural phenomena, and limiting the number of empirically-determined parameters to a manageable number through analysis of experimental shear/torsion tests.

Two-Phase Model

In the two-phase model (Stone and Rashid, 1994), an attempt is made to mathematically represent the effects of the phase-region size in the tin-lead alloy. As discussed in the introduction, the characteristic size of the lead-rich phase regions (the Sn-rich as well) has been observed to correlate strongly with strain localization and subsequent failure. In particular, local phase-region coarsening appears to be accompanied by a decrease in the overall flow resistance of the material, leading to an unstable concentration of strain and, ultimately, to fracture. Whereas the model is intended to represent the effects of this coarsening phenomenon, the behavior of individual phase regions is not explicitly accounted for. In "microstructurally motivated" material models such as this one, the model predictions are envisaged to correspond to a representative volume element of material that contains a statistically meaningful distribution of microstructural features. In concept, then, the physical material, with all its microscale heterogeneities, is represented by a replacement medium in which the important microstructural features (in this case, lead-rich phase regions) are present only in the material model itself. The material model involves state variables that characterize some statistical measure of the microstructure, and which generally vary smoothly in space. It is emphasized that the idea of a representative volume element does not constitute an analytical ingredient in a model of this type; rather, it is a conceptual guide in the model formulation.

The two-phase model retains separate average stress tensors $\mathbf{T}^1$ and $\mathbf{T}^2$ in the lead-rich and tin-rich phases, respectively. The average volumetric response for each phase is given by $\dot{p}_\alpha = -K_\alpha tr\underline{D}$ where p_α is the pressure of phase $\alpha = 1,2$ defined by the negative of one-third the total stress tensor, $\underline{D}$ is the imposed stretching rate (i.e., symmetric part of the spatial velocity gradient), and K_α is the bulk modulus of the α phase. Taking all subsequent rank-two tensors as deviatoric (without prime), each is governed by the evolution equation:

$$\boldsymbol{T}^{\circ\alpha} = 2G_\alpha(\boldsymbol{D} - \mu_\alpha \boldsymbol{T}^\alpha) \qquad \text{Eqn. (5)}$$

in which $\boldsymbol{T}^\circ$ indicates the Jaumann corotational rate, G the elastic shear modulus (elastic response taken to be isotropic), **D** the imposed stretching rate (i.e. symmetric part of the spatial velocity gradient), and α=1 (Pb-rich) or 2 (Sn-rich) specifies the phase. The overall Cauchy stress for the material element is obtained from the simple volume-average relation

$$\boldsymbol{T} = f\boldsymbol{T}^1 + (1-f)\boldsymbol{T}^2 \qquad \text{Eqn. (6)}$$

in which f=0.40 and is the volume fraction of the lead-rich phase. Equations (5) and (6) represent the simplest possible means of modeling a mixture of two inelastic phases: each phase is assumed to exhibit simple isotropic viscoplastic behavior and experience an identical imposed deformation rate, and the overall stress is obtained through a simple volume-weighted average. Any departure from these assumptions would involve considerable complication that is not warranted in this context.

The flow-rate parameters μ_α are taken to be given by the power-law expression:

$$\mu_\alpha = \frac{\dot{\varepsilon}_0}{\tau_\alpha}\left(\frac{\tau_\alpha}{\sigma_\alpha}\right)^{\frac{1}{M_\alpha}} \qquad \text{Eqn. (7)}$$

In (7), $\tau_\alpha = (T^\alpha_{ij}T^\alpha_{ij})^{1/2}$ is the magnitude of the stress in each phase, $\dot{\varepsilon}_0$ is a constant with units inverse time, and M_α is the rate-dependence exponent in each phase. The terms σ_α are the values of the flow resistance in each phase, and are themselves subject to evolution laws that govern the hardening or softening behavior. In particular:

$$\sigma_\alpha = (\bar{\sigma}_\alpha + \hat{\sigma}_\alpha)\,\sigma^0_\alpha \qquad \text{Eqn. (8)}$$

$$\dot{\bar{\sigma}}_\alpha = C^\alpha_1 \frac{\dot{\gamma}_\alpha}{\dot{\varepsilon}_0} - C^\alpha_2 \left(\frac{\dot{\gamma}_\alpha}{\dot{\varepsilon}_0}\right)^{n_a} \bar{\sigma}_\alpha \qquad \text{Eqn. (9)}$$

$$\hat{\sigma}_\alpha = C^\alpha_3 \left(\frac{\lambda}{\lambda_0}\right)^{-\frac{1}{2}} \qquad \text{Eqn. (10)}$$

$$\dot{\lambda} = \lambda_0 \left[f C^1_4 \dot{\gamma}_1 + (1-f)\, C^2_4 \dot{\gamma}_2\right] \qquad \text{Eqn. (11)}$$

in which $\dot{\gamma}_\alpha \equiv \mu_\alpha \tau_\alpha$ (equivalent plastic strain rate in each phase). In (8) - (11), C^α_1, C^α_2, C^α_3, C^α_4, M_α, σ^0_α, n_α, $\dot{\varepsilon}_0$ and λ are material constants, whereas λ, $\bar{\sigma}_\alpha$, and $\hat{\sigma}_\alpha$ are state variables. The term $\bar{\sigma}_\alpha$ is intended to quantify the contribution of the dislocation network to flow resistance and is therefore made to evolve with inelastic deformation; its evolution equation is written in hardening-recovery format as in Rohde and Swearengen (1980) and Busso et al. (1992). The term λ is a characteristic length associated with the phase-region size; its evolution equation is also related to a scalar measure of inelastic deformation rate as suggested by Arrowood et al. (1991). The parameter $\hat{\sigma}_\alpha$ is defined directly by the Hall-Petch relationship, and is intended to quantify the effects of disruption of dislocation glide due to finite crystallite size.

Equations (5) - (11) completely specify the two-phase constitutive model. This model has been implemented in a three-dimensional, large-deformation finite element code (JAC3D), and has been used to simulate experiments performed on the tin-lead near-eutectic solder alloy. A few of the results of these studies are presented below.

Thermomechanical fatigue tests were performed to examine the microstructural evolution and mechanical behavior of the solder joints. Hysteresis loops of one thermomechanical fatigue test for 10% shear strain at a strain rate of $2.8\text{x}10^{-4}\text{sec}^{-1}$ is shown in Figure 10. A plot of a single hysteresis loop (after 10 cycles) is shown in Figure 11. A plot of the deformation behavior as a function of each cycle is shown in Figure 12. In this plot the high temperature load corresponds to the maximum load on the hysteresis loop at 125°C, the relaxed load corresponds to the load after the 3 minute hold at 125°C, and the low load is the load on the hysteresis loop at -55°C. In this plot the

load begins to decay at about 225 cycles, which is also the time at which electrical opens are detected in the sample. This is when failure is defined to occur. The other tests performed on this alloy, under these conditions, resulted in very similar mechanical behavior, so duplicate results are not given in this report. An example of the microstructural evolution in the 60Sn-40Pb solder joints was shown previously in Figure 3. A detailed view of the coarsened band with a crack present is shown in Figure 13 (failed sample after 300 cycles). The crack initiates in the coarsened band at the Sn-Sn grain boundaries and then propagates intergranularly through the Sn-rich phase the Sn grain boundaries (Frear, 1992).

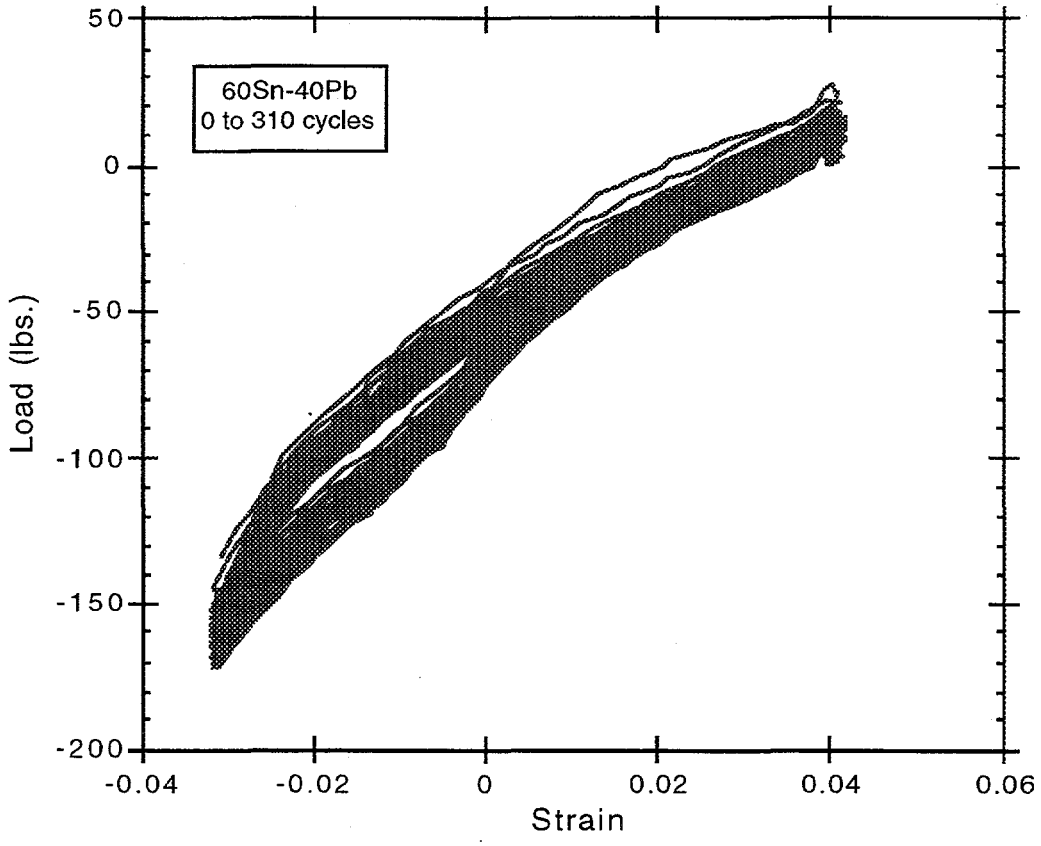

Figure 10 Hysteresis loops of a 60Sn-40Pb solder joints after 310 cycles between -55 and 125°C.

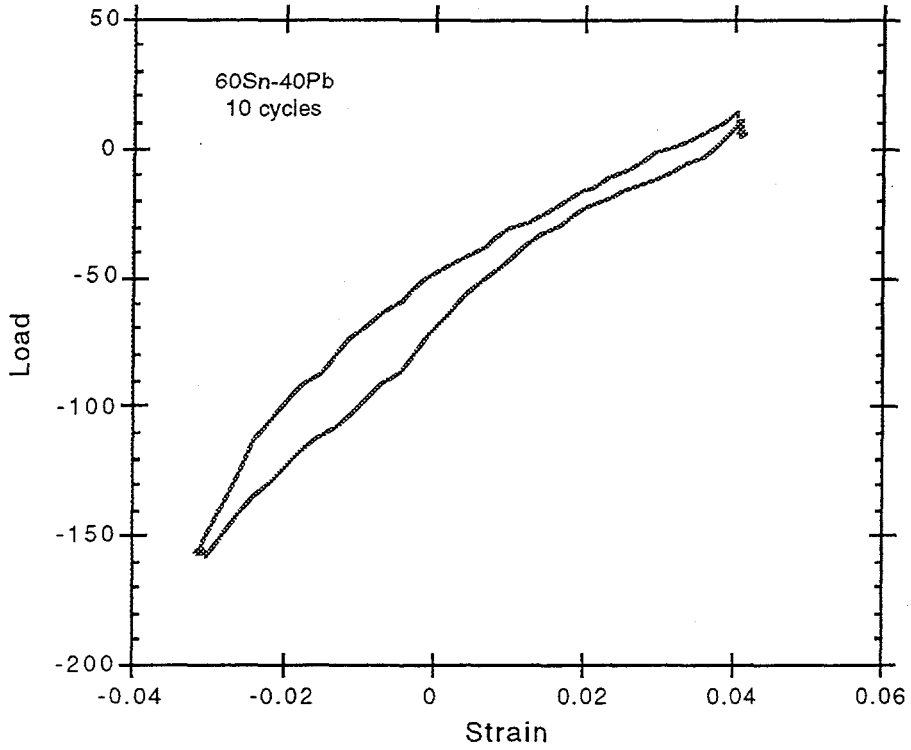

Figure 11 Hysteresis loop of 60Sn-40Pb solder joints after 10 thermal cycles between -55 and 125°C

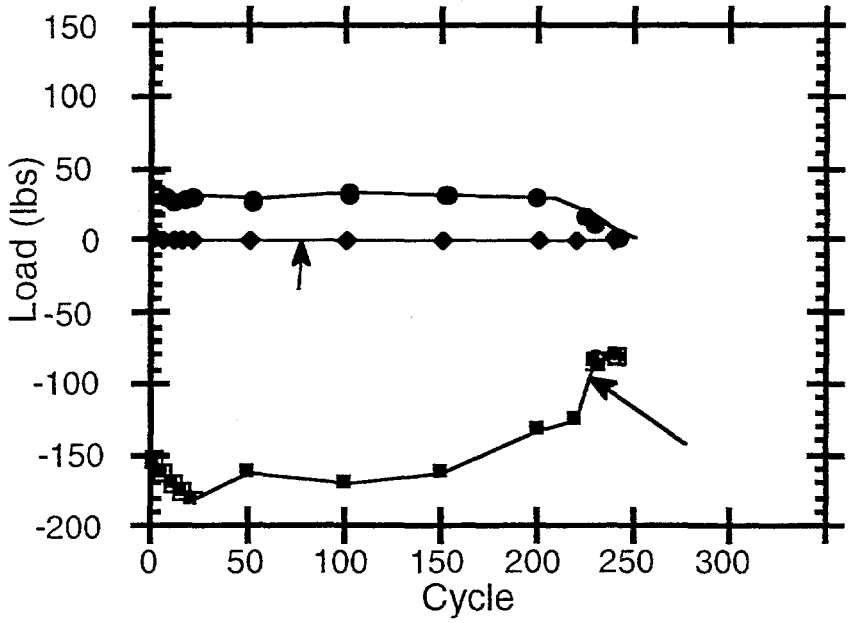

Figure 12 Plot of load versus number of thermal cycles for the extremes of the hysteresis loops.

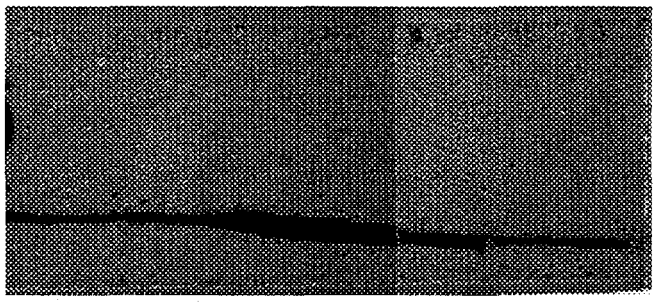

Figure 13 Failed 60Sn-40Pb solder joint after 300 cycles between -55 and 125°C. The crack has formed in the coarsened band in the solder microstructure.

The results of *in situ* thermomechanical fatigue tests (-25 125°C and 10% total shear strain) are shown in Figure 14. Figure 14A is the as-solidified microstructure and 14B shows the structure after 25 cycles. Even after 25 cycles the solder microstructure has coarsened at the cell boundaries. The dark lines at the cell boundaries in Figure 14B are not cracks, they are artifacts of surface roughness. As the solder microstructure deforms, the individual cells slide and rotate at the cell boundaries to accommodate the strain because the boundaries are the weakest part of the microstructure (Frear,1992). Observations by Lee (1993) showed that the surfaces of solder joints in electronic assemblies that have undergone thermomechanical fatigue revealed the sliding of eutectic cells and some surface crack initiation at the cell boundaries. These results show that constitutive models developed to predict near eutectic Sn-Pb solder joint behavior must include dynamic microstructural evolution.

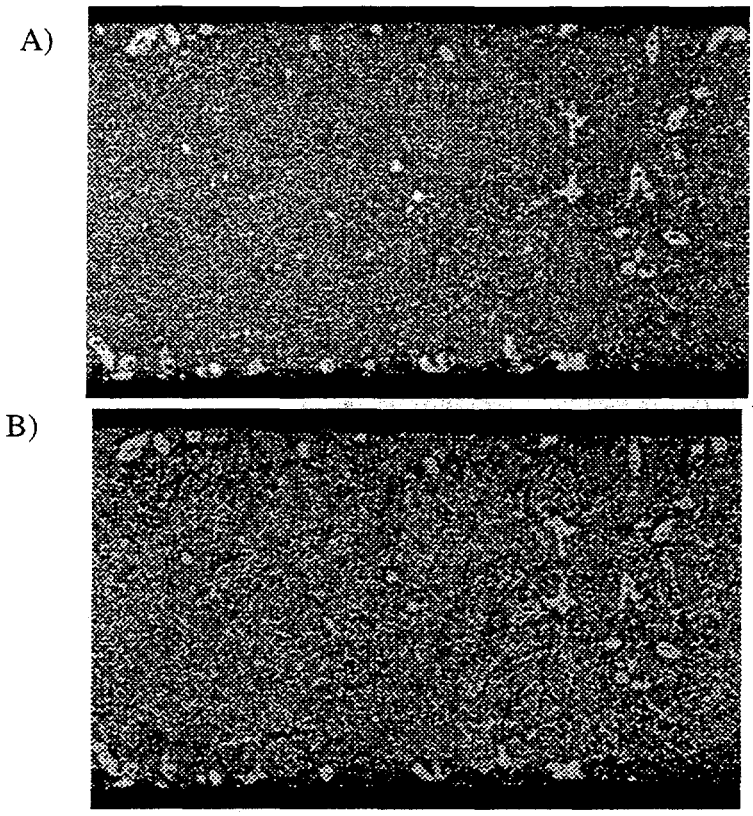

Figure 14 SEM micrographs of a solder jounnt using the *in situ* thermo-mechanical fatigue system. A) As solidified joint, B) after thermal

Examples of solder joints that have been thermomechanically fatigued, using the test geometry described above are shown in Figures 15 and 16. Both were tested at 10% shear strain at -55° to 125°C for 100 cycles. The sample in Figure 15 was tested at a deformation rate of $5.6x10^{-4}$ s^{-1}, and the sample in Figure 16 was tested at a deformation rate of $2.1x10^{-4}$ s^{-1}. In Figure 15, the heterogeneous coarsened microstructure occurs adjacent to the bottom interface. In Figure 16, heterogeneous coarsening occurs throughout the microstructure at the cell boundaries. The cause of this difference in microstructural evolution is due to the deformation rate sensitivity of the solder joint. At the faster deformation rates ($>5.6x10^{-4}s^{-1}$), the strain is not accommodated primarily at the colony boundaries but at a region in the solder joint where there is a stress concentration parallel to the direction of imposed shear strain. In this case, the deformation is imparted to the solder too quickly to be accommodated at the colony boundaries, by colony sliding and rotation, and is imposed to a thin region in the solder joint where there is a stress concentration. The faster deformation rates have a shorter lifetime because the strain is concentrated into a much thinner region of the joint, rather than at colony boundaries, which accelerates the coarsening process and leads to a more rapid failure.

To illustrate the effects of microstructural coarsening and to correlate with the experimental results discussed above (Figures 14-16), an example calculation was performed on a test specimen representative of a simulated solder joint, (Figure 17). In this three-dimensional simulation, the 60Sn-40Pb solder was constrained between two copper platens which were modeled as elastic bodies. The cyclic shear displacement, defined in Figure 18, was applied to the top surface of the upper

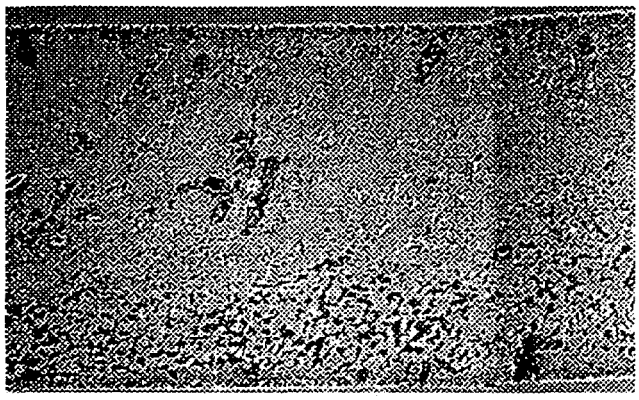

Figure 15 60Sn-40Pb solder microstructure after 100 thermal cycles and 10% shear strain and a deformation rate of $5.6x10^{-4}s^{-1}$.

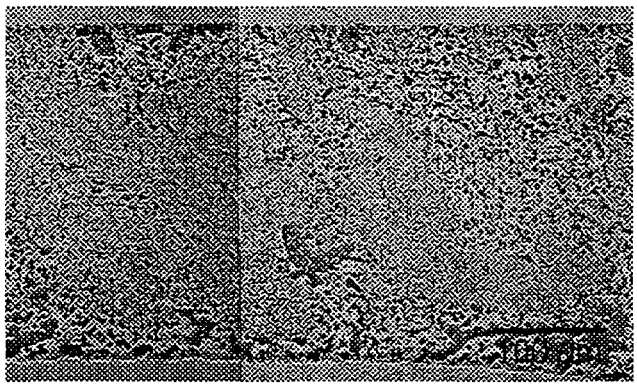

Figure 16 60Sn-40Pb solder microstructure after 100 thermal cycles and 10% shear strain and a deformation rate of $2.1x10^{-4}s^{-1}$.

copper platen while the bottom surface of the lower platen was restrained. The shear displacement approximates deformation due to thermal cycling in a typical solder joint, although the computation is isothermal. The magnitude of the shear displacement translates to approximately +/- 5% (total strain range =10%) shear strain in the solder joint. The strain rate assumed was $2.0x10^{-4}$/in. The material properties used for the two phase constitutive model discussed earlier are given in Table 2. The material constants used in the analysis were λ_0=1.0μm, $\dot{\varepsilon}_0$=1.0min^{-1}, and f=0.4.

Table 2: Material Properties

Parameter	Lead-rich Phase	Tin-rich Phase
G	6.9 Gpa	13.8Gpa
B	15.2Gpa	30.3Gpa
M	0.3	0.1

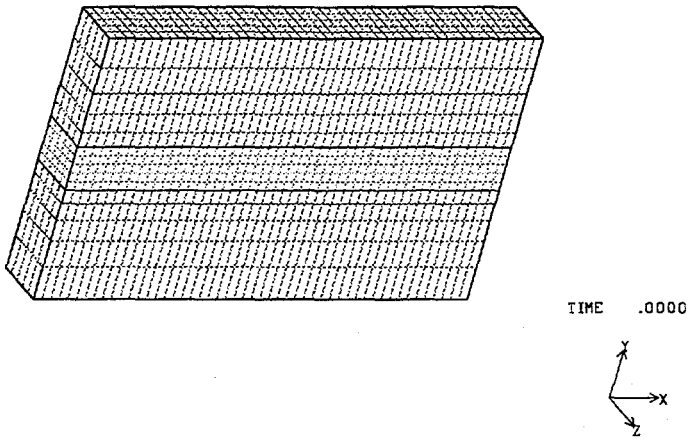

Figure 17 Meshed solder joint for two phase finite element simulation

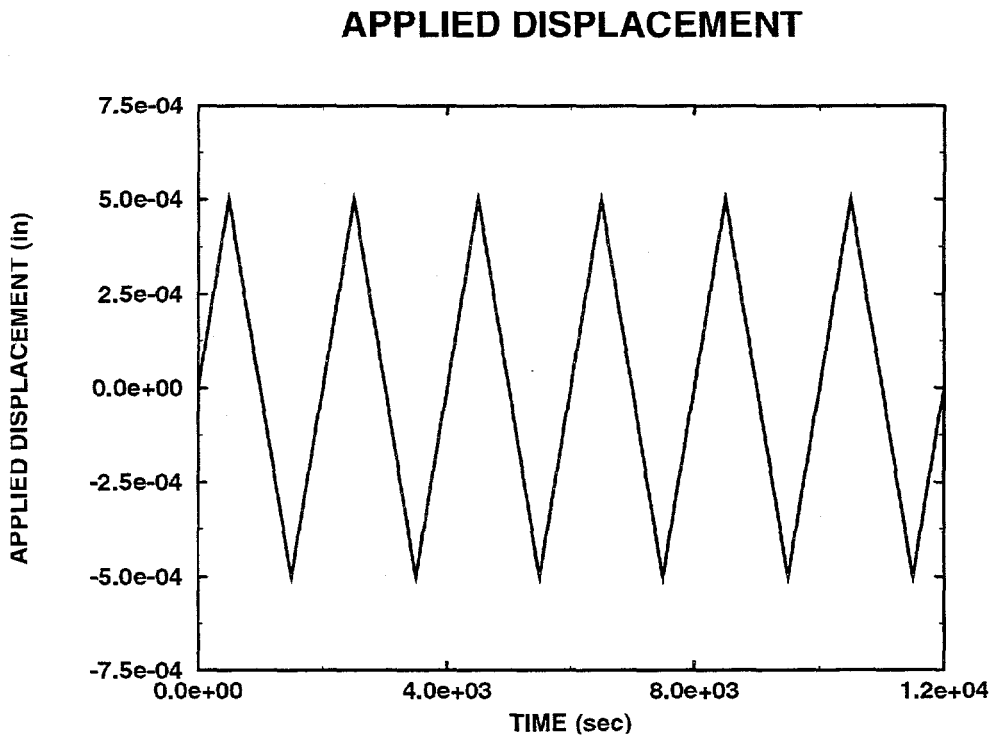

Figure 18 Applied displacement versus time used for the two-phase finite element simulation.

Table 2: Material Properties

Parameter	Lead-rich Phase	Tin-rich Phase
σ^0	6.9Mpa	13.8Gpa
C_1	20.0	20.0
C_2	100.0	100.0
C_3	1.0	1.0
C_4	10.0	10.0

Two computations were completed. In the first computation, the microstructure was assumed to initially be perfectly uniform, $\lambda_0 = 1.0\ \mu m$ everywhere. In Figure 19, the phase-size parameter, λ, is plotted at the end of six complete cycles. The results of this computation shows two bands where the microstructure coarsens; a dominant coarsened band near the top platen and a minor band near the bottom platen. At these locations, the material softens and strain is localized. These results compare favorably with observed microstructural coarsening for this geometry. The coarsening in this computation is precipitated by the shear strain variations in the solder.

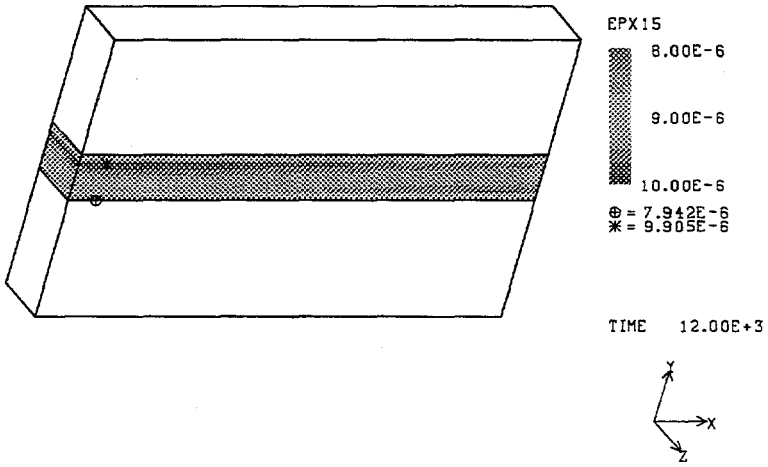

Figure 19 Finite element simulation results after 6 cycles for a uniform initial microstructure. Note that the heterogeneous coarsening occurs near the solder/copper interfaces.

In the second computation, the microstructure was assumed to be initially coarsened in the center of the solder joint. After six displacement cycles, the microstructural coarsening and strain localization in the center of the solder joint is substantially enhanced, as shown in Figure 20.

In Figure 21, the maximum phase-size parameter, at the end of six complete cycles, λ, is plotted as a function of time for the two simulations described above. The effect of initial microstructure is substantial. If one assumes that initial crack formation of the solder joint can be related to a specific grain size, the number of cycles to develop initial cracking would be substantially different,

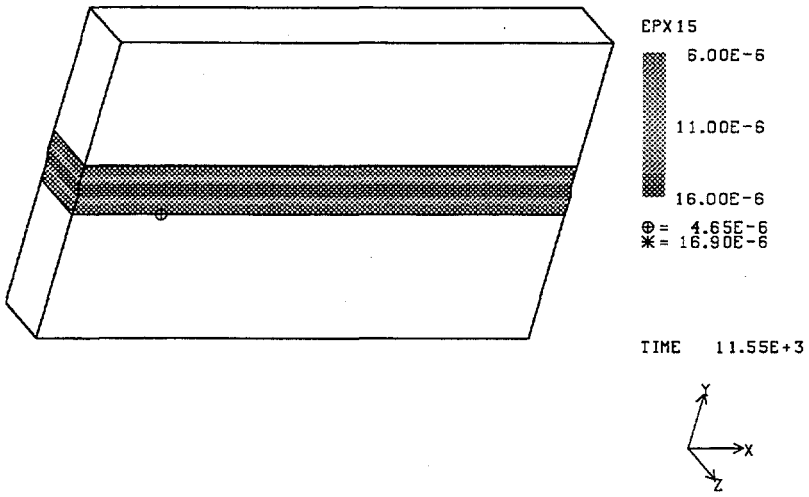

Figure 20 Finite element simulation results after 6 cycles for a microstructure with an initial coarsened structure in the center of the joint.

depending upon initial microstructure. The number of cycles to failure would be substantially greater if no initial coarsened band was present in the as solidified microstructure. It must be stated that the material properties and parameters used in the simulations have not been adequately fit to 60Sn-40Pb solder and the model at the present time is not temperature dependent. These computations do, however, indicate that the two-phase model simulates the microstructural response of solder joints in thermomechanical fatigue conditions.

Despite the numerous simplifications and assumptions that have been made in arriving at the two-phase model, it is clear that experimentally obtaining reliable values for the constants that appear in the model is a formidable task. In particular, it is unclear if values for the constants corresponding to the individual phases can be obtained from either tests performed on the pure elemental phases or the mixture itself. As mentioned previously, however, the role of this model is that of research tool: even without accurate estimates for the material parameters, the model is of some utility in assessing the validity of various failure-sequence hypotheses through numerical experimentation.

Single-Phase Model

In this model, no attempt is made to explicitly account for the microstructural coarsening effect. Rather, the simplest possible forms are chosen for the evolution equations in the model such that the important features of inelastic flow in the tin-lead near-eutectic alloy are represented. These forms are, in a sense, motivated by microscale considerations; however, this model's connection to microstructural observation is more tenuous than that of the previous model. The result is a model for which material parameter values can be reliably obtained from tests, and whose utility lies in facilitating engineering predictions made on the basis of finite element computations.

The single-phase model is based on the isotropic stress evolution equation:

$$\boldsymbol{T}^{\circ} = 2G\,(\boldsymbol{D} - \mu\boldsymbol{T}) \qquad \text{Eqn. (12)}$$

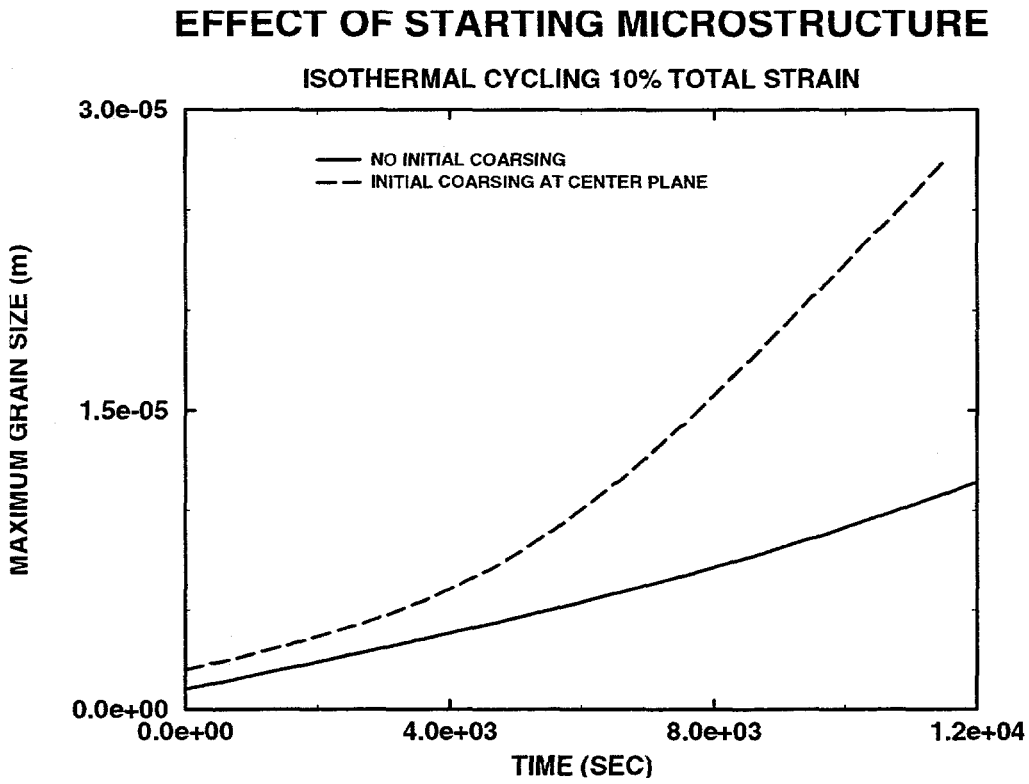

Figure 21 Plot of maximum grain size versus time for the finite element simulations that shows that an initially coarsened microstructure rapidly produces additional heterogeneous coarsened regions.

which is identical in form to that used in each phase in the two-phase model. In constructing the flow rate function μ, and in particular the manner in which it represents hardening, the following items were considered:

- Inelastic flow in the alloys of interest, and in the temperature and strain-rate ranges of interest, is primarily due to dislocation motion, with relatively small contributions from diffusional mechanisms.

- Hardening is due to barriers to dislocation motion, such as immobile dislocations and phase-region boundaries.

- The overall resistance to dislocation motion offered by the current pattern of barriers embodies the state of hardening; in this model it is quantified by a single scalar state variable.

- Any real distribution of barriers is heterogeneously distributed on the submicron scale. For instance, immobile dislocations may organize themselves into a cellular structure, with cell interiors that are relatively free of dislocation debris. Certainly the arrangement of phase-region boundaries has a definite geometric structure. Accordingly, mobile dislocations will interact with these obstacles in a directionally-dependent manner. In particular, mobile dislocations may pile up against barriers, and when the stress direction is changed (or reversed), the resistance experi-

enced by these piled-up dislocations may be significantly reduced. With regard to plasticity modeling, the usual conception of kinematic hardening involves the modification of the stress by subtracting from it a back stress, and then using the modified stress in a yield criterion or flow relation. This formulation corresponds most closely to grain-scale residual stresses as the mechanism responsible for directional hardening, as in metals at low homologous temperatures. However, in the case of solder, and more to the point, the high homologous temperatures at which it is used, it seems that large residual stresses on a small scale would relax quickly. Accordingly, the directional hardening is represented here as a modification to the isotropic flow resistance (i.e. the scalar hardening state variable mentioned above) rather than as a modification to the stress tensor itself. Indeed, this model is consistent with a simplified picture of the microscopic processes, in which the entire mobile dislocation network is subjected to a uniform stress. This network, however, may be interacting with the pattern of obstacles in a directional manner, due to pile-ups.

- Due to thermal activation and the dislocation-scale interaction stresses, both the immobile dislocation network, and any pile-ups of mobile dislocations, will tend to recover over time. The rate of recovery is enhanced by the application of stress. In the presence of stress, the recovery processes compete with the hardening processes.

The equations given below that define the scalar inelastic flow rate are the simplest possible forms that are consistent with the above qualitative statements. Whereas a "rigorous derivation" of a set of evolution equations based on the ideas listed above is, of course, not to be expected, it is important that the final model render predictions that are at least consistent with these assumed underlying mechanisms. The chosen form for the scalar inelastic deformation rate is:

$$\gamma = \varepsilon_0 \sinh^m\left[\frac{\tau}{\alpha\Gamma\sigma}\right] \qquad \text{Eqn. (13)}$$

$$\dot{\sigma} = A_1\dot{\gamma} - A_2(\sigma - \sigma_0)\,(1 + A_3\gamma) \qquad \text{Eqn. (14)}$$

$$\Gamma = 1 + \frac{\boldsymbol{T}}{\tau} \bullet \boldsymbol{B}$$

$$\dot{\boldsymbol{B}} = \dot{\gamma}\left(A_4\frac{\boldsymbol{T}}{\tau} - A_5\boldsymbol{B}\right) - A_6\boldsymbol{B} \qquad \text{Eqn. (15)}$$

In (13) - (15), $\gamma = \mu/\tau$ is a scalar measure of inelastic flow rate, and α depends only on temperature. The rate-dependence relation (13) involves a hyperbolic sine function raised to a power, which was successfully used to fit a large amount of data by Darveaux and Banerji (1992). Consistent with the above discussion of dislocation pile-ups and the associated directionality of hardening, the scalar flow resistance is scaled by Γ, which is unity in the absence of directional hardening. The directional hardening is represented by the symmetric rank-two tensorial state variable **B** (similar to a back stress), which obeys the evolution equation given in (15). In the case of persistent unidirectional loading, **B** is coaxial with the Cauchy stress, and saturates at a value of $(A_4/A_5)\mathbf{T}/\tau$ for fast loading processes. For lower strain rates, the A_6 term in (15) (i.e. the recovery term) competes with the growth of **B**. In general, (15) is written so that **B** always tends toward the prevailing stress direction, and at a rate proportional to the inelastic flow rate, but with a recovery term that generally

decreases the magnitude of **B**. The recovery can proceed in the absence of stress so long as the temperature is high enough, as it does in reality. Γ as given in (15) measures the extent to which **B** and the current stress are coaxial, and is used in (13) to modify the flow resistance that is experienced by the current pattern of mobile dislocations under the current stress state.

The first term in the evolution equation (14) for the scalar hardening parameter is a (linear) hardening term. The second term is a recovery term that competes with (and diminishes) the hardening in a nonlinear fashion. The σ_0 is the annealed (or long-time-unstressed) flow resistance, and the term $A_2(\sigma-\sigma_0)$ is the rate of recovery due to the dislocation interaction stresses. This rate of recovery can be accelerated by the application of stress (producing an inelastic flow rate), giving rise to the $A_3\gamma$ term.

The material parameters are A_1 - A_6, σ_0, ε_0, m, α, and two elastic constants (G and K). All of these constants are expected to be functions of temperature. At room temperature α was set to unity, whereas ε_0 was taken to be $1.0\text{x}10^{-4}$ sec^{-1}. A room-temperature value of m=3.3 taken from the work of Darveaux and Banerji (1992), as was the shear modulus G= $1.3\text{x}10^4$ MPa ($1.9\text{x}10^6$ psi). The parameters A_1 - A_6 and σ_0 were obtained by fitting the predicted stress response to the measured stress history in the tube-and-plug-type material test as described earlier. In this test, a thin (0.254mm (0.010")) annular region of solder fills the gap between a tube and a plug, which may be subjected to a combination of shear and torsion. These two modes of deformation subject the sample to shear deformation in orthogonal directions. A plot of the resultant load (loading on the z-axis of the specimen) and torque (rotational loading) as a function of the deformation cycle is shown in Figure 22. For the purposes of obtaining the required seven parameters the program of deformation in Table 1 was used.This pattern was repeated for a total of five cycles. This particular deformation path was chosen in order to probe not only the isotropic hardening behavior, but the directional hardening response as well. The deformation rates were specified so that the strain amplitude in each direction was roughly 0.05.

Because the stress response depends on the unknown parameters through the rate equations given above, the values of the parameters may not be obtained simply by, say, measuring a slope of a stress-strain curve. Indeed, the stress history over the entire deformation path depends on each of the parameters in a complex and highly coupled fashion. Accordingly, a conjugate-gradient-search procedure was used to aid in determining the values of the constants from the test data. In this procedure, a norm **I** is defined as:

$$\boldsymbol{I} = \int_{t_1}^{t_2} \sqrt{(T_{13}-S_{13})\,(T_{13}-S_{13}) + (T_{23}-S_{23})}\,dt \qquad \text{Eqn. (16)}$$

which provides a scalar measure of the difference between the measured components of the experimental stress deviator **S**, and the computed stress deviator **T**. The gradient of **I** with respect to the seven unknown constants is computed by means of a perturbation technique. This gradient is subsequently used in a conjugate gradient algorithm to minimize the difference function **I**. In this way, the following values for the material constant were obtained (valid at room temperature):

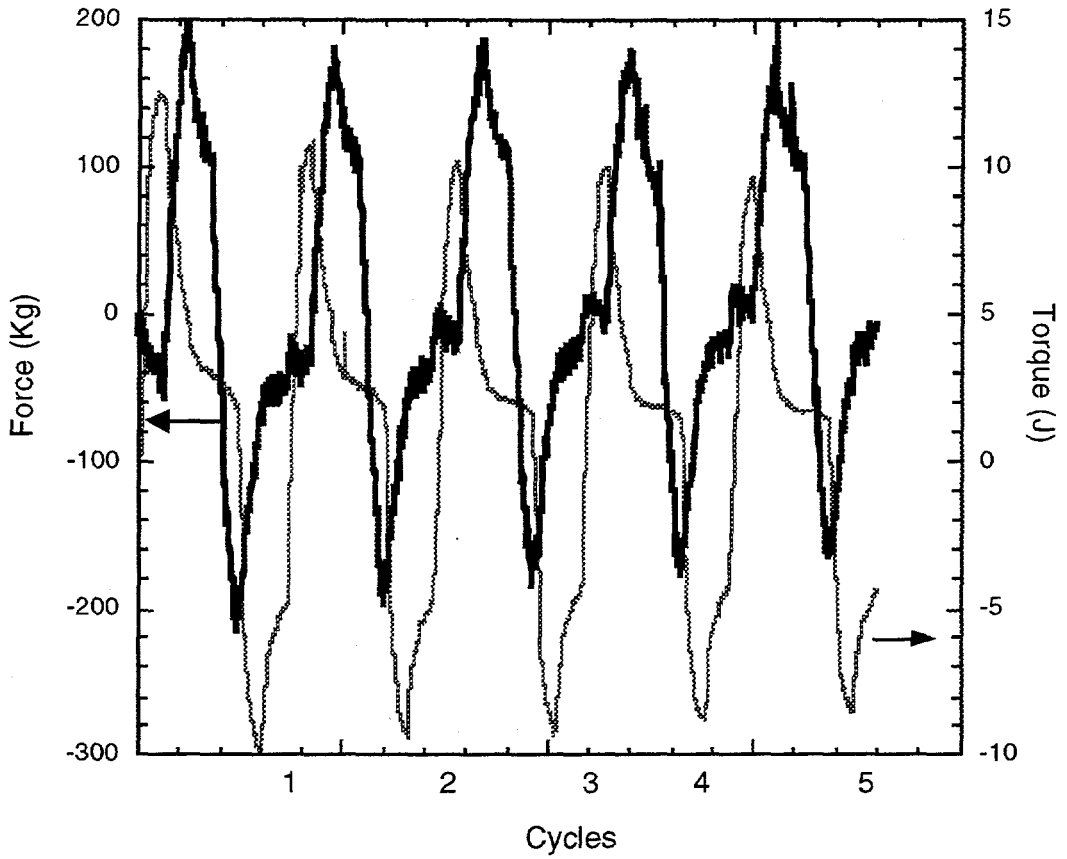

Figure 22 Plot of force and torque versus number of cycles on the shear/torsion specimen.

σ_0=3930 psi, A_1=-1.261 psi, A_2=-9.16x10^{-4}s^{-1}

A_3=1.33x10^{-3}s^{-1} A_4=2.20, A_5=0.218, A_6=1.50x10^{-4}s^{-1}

These parameter values resulted in the fit shown in Figure 23, in which the solid lines are the experimental stress histories for both shear and torsion (also seen in Figure 22) and the dashed lines are the computed stress histories. The experimental curves were piece-wise fit using a third-order polynomial to determine the material constants for the single-phase model. The discrepancies observed during relaxation and unloading seem to arise from use of the Mises-type isotropic flow rule. Currently, various alternatives are being studied to improve the fit in these regimes.

Conclusions and Recommendations

The purpose of this project was to develop constitutive models for solder joints under strain and temperature cycling conditions, taking into account the microstructural heterogeneities that exist in as-solidified near eutectic Sn-Pb joints as well as subsequent microstructural evolution. These models were then implemented in the JAC3D finite element code and used to simulate the response of solder joint test specimens under strain and temperature cycles. The computational effort was tightly coupled with the experimental work, with respect to material data measurement, initial mi-

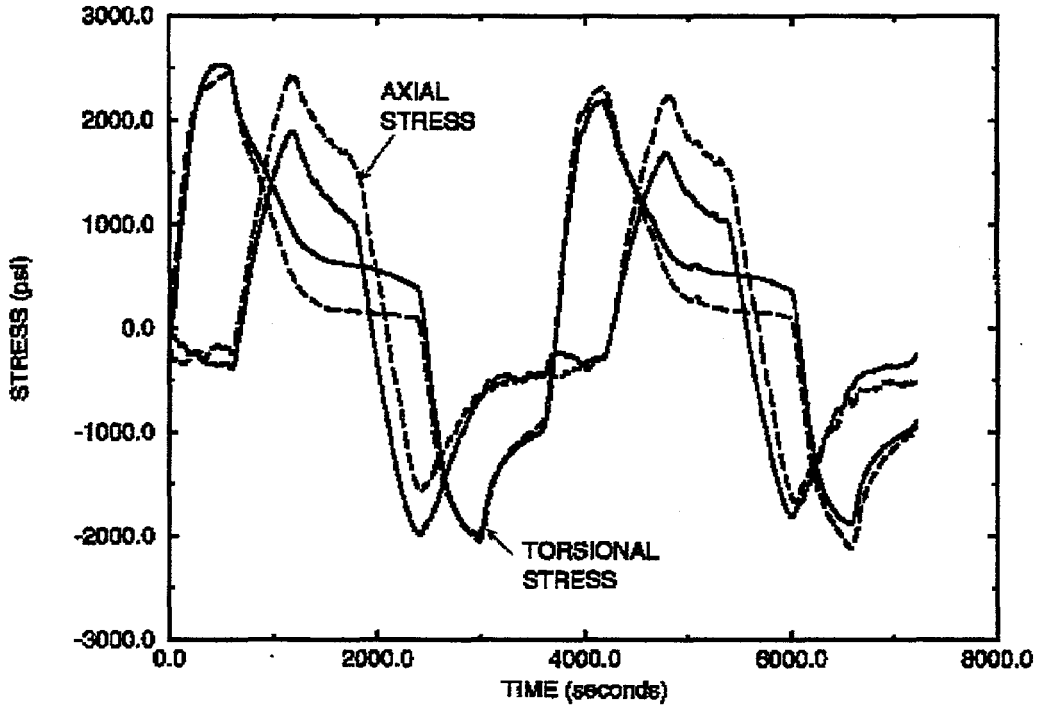

Figure 23 Plot of experimental shear/torsion test results with an overlay of the single-phase model prediction.

crostructural characterization, and imposed thermomechanical history.

In this report, methodologies have been presented that use simplified experimental tests as fundamental input for two different constitutive models to predict the behavior of solder joints under conditions of thermomechanical fatigue.

The two phase model mathematically represents the effects of the phase-region size in the 60Sn-40Pb solder alloy and predicts the heterogeneous coarsening phenomenon of near-eutectic Sn-Pb solder under conditions of fatigue. Results using the two-phase model code showed good correlation with metallurgical experiments, and subsequently showed that the presence of an initial heterogeneity in the solder microstructure accelerates the development of coarsening and could significantly reduce the fatigue life. The difficulty with this model is that deriving the material constants needed for the constitutive relations is a formidable task; in particular it is not clear whether the constants for the individual phases can be reliably obtained from tests on either the independent elemental materials or the mixture itself. However, this model has utility in assessing the validity of failure-sequence events of solder thermomechanical fatigue where microstructural evolution dominates failure.

The single-phase model was developed to predict the mechanical behavior, and eventually reliability, of solder joints using materials data that is readily available through metallurgical experiments. This technique could be very useful for conditions where microstructural evolution is not a domi-

nant factor in fatigue. A shear/torsion test sample was developed to impose shear strains in two different orientations to a solder joint. Constitutive relations were derived whose material constants could be determined by fitting them to shear/torsion test data. The predicted behavior shows adequate fit to the experimental results and various alternatives are being explored to develop a better fit. The promise shown in this technique is that the material constants needed for constitutive behavior input to finite element simulations may be determined through a series of easily performed experimental tests. This would thereby simplify the effort needed perform lifetime prediction through use of this engineering methodology.

The constitutive models show a great deal of promise as a methodology to determine the behavior of solder joints under conditions of thermomechanical fatigue in order to make reliability predictions without the need for extensive testing. However, using these complex models requires mechanics and materials expertise and computing resources beyond that generally available to designers of electronic packages. A natural continuation of this project would be to develop model reduction techniques that retain the fundamental physical behavior of the solder in a format that is immediately useful in design.

References

Akay, H. U., Tong, Y., Paydar, N., 1993, "Thermal Fatigue Analysis of a SMT Solder Joint Using a Nonlinear FEM Approach", J. Microcircuits and Electron. Packaging, vol. 16, pp. 79-88.

Arrowood, R., A. Mukherjee, and W. B. Jones, in Solder Mechanics: A State of the Art Assessment, D. R. Frear, W. B. Jones, and K. R. Kinsman, eds., p. 107, The Minerals, Metals, and Materials Society, 1991.

Burchett,S.N., 1991, "Stress Analysis of a Leadless Chip Carrier Soldered to a Ceramic Substrate", ASME Winter Annual Meeting, Dec. 1-6,1991,Atlanta,Ga.,91-WA-EEP- 1.

Busso, E. P., Kitano, M., Kumazawa, T., 1994, "Modeling Complex Inelastic Deformation Processes in IC Packages' Solder Joints", J. Electron. Packaging, vol. 116, pp. 6-15.

Busso, E. P., M. Kitano, and T. Kumazawa, "A visco-plastic constitutive model for 60/40 tin-lead solder used in IC package joints," J. Eng. Mat. Tech.,114, p. 331, 1992.

Charles,H.K.,Jr and Clatterbaugh, G.V., 1990, "Solder Joint Reliability -- Design Implications from Finite Element Modeling and Experimental Testing,"ASME Journal Electronic Packaging, Vol. 112,No.2, pp. 135-146.

Clech, J-P., Englelmaier, 1989, W., Kotlowicz, R. W. and Augis, J. A., SMART Conf. V, New Orleans, LA.

Coffin, L. F., 1971, J. Mater., vol. 6, pp. 388-402.

Coffin, L. F., Jr., 1969, Fracture 1969, Chapman and Hall, London.

Coffin,L.F.Jr., 1954, Trans. ASME V76, pp.931-950.

Darveaux, R., and K. Banerji, "Constitutive relations for tin-based solder joints," IEEE Trans. Components, Hybrids, and Manufacturing Tech.,15, pp. 1013-1024, 1992.

Dasgupta, A., Oyan, C., Barker, D., Pecht, M., 1992, "Solder Creep-Fatigue Analysis by an Energy-Partitioning Approach", J. Electron. Packaging., vol. 114, pp. 152-160.

Frear, D. R., 1992, "Microstructural Evolution During the Thermomechanical Fatigue of Solder Joints", in The Metal Science of Joining, Cieslak, Glicksman, Kang and Perepezko eds., TMS Publications, 191-200.

Frear, D. R., 1989, "Thermomechanical Fatigue of Solder Joints: A New Comprehensive Test Method" IEEE Comp. Hybrids. Manufact. Tech., CHMT–12, pp. 492–501.

Frear, D. R., 1989, IEEE Comp. Hybrids. Manufact. Tech., CHMT–12 ,pp. 492–501.

Frear, D. R., Rashid, M. M., Burchett, S. N., 1993, "Microstructurally Based Thermomechanical Fatigue Lifetime Model of Solder Joints for Electronic Applications", Reliability, Stress Analysis and Failure Prevention, DE-vol. 55, ASME, R. J. Schaller, ed., pp. 277-287.

Frear, D. R., Burchett, S. N., Rashid, M. M., 1995, "A Microstructurally Based Model of Sodler Joints Under Conditions of Thermomechanical Fatigue", Proc. InterPack'95, ASME.

Guo, Q., Cutiongco, E. C., Keer, L. M., Fine, M. E., 1992, "Thermomechanical Fatigue Life Prediction of 63Sn-37Pb Solder", J. Electron. Packaging, vol. 114, pp. 145-151.

Hacke, P., Sprecher, A. F., Conrad, H., 1993, "Computer Simulation of Thermomechanical Fatigue of Solder Joints

Including Microstructure Coarsening", J. Electron. Packaging, vol. 115, pp. 153-158.
Huang, J. H., Pei, J. Y., Qian, Y. Y., Jiang, Y. H., 1994, "Life Predictions of SMT Solder Joints under Thermal Cycling", Soldering and Surface Mount Technol., vol. 16, 31-50.
Jones,R.E., 1974, "QMESH:A Self-Organizing Mesh Generation Program," SLA-73-1088, Sandia National Laboratories Albuquerque,NM.
Lau, J. H. and Harkins, G., 1988, "Thermal-Stress Analysis of SOIC Packages and Interconnections", Proc. IEEE 38th ECC Conf., 38, p. 23-31.
Lau, J. H., 1993, "Thermal Fatigue Life Prediction of Flip Chip Solder Joints by Fracture Mechanics Method", Engineering Fracture Mechanics, vol. 45, pp. 643-654.
Lau, J., Erasmus, S., 1993, "Reliability of Fine Pitch Plastic Quad Flat Pack Leads and Solder Joints Under Bending, Twisting, and Thermal Conditions", J. Electron. Packaging, vol. 115, pp. 322-328.
Lau.J.H.,and Rice,D.W., 1986, "Effects of Interconnection Geometry on Mechanical Responses of Surface Mount Component," PROC.,2nd IEEE International Electronic Manufacturing Technology Symposium, San Francisco, CA, pp.205-217.
Lee, S. M., 1993, "Creep and he Creep-Fatigue Interaction in Pb-Sn Eutectic and Eutectic Solder Joints", Ph.D. Thesis, The University of Wisconsin, Madison.
Lee, S. M., Stone, D. S., 1990, Proc. 40th IEEE ECTC Conf., Las Vegas, NV,p. 491.
Liedtke,P.E., Heinrich,S.M., Elkouh,A.F., Nigro,N.J. Lee,P.S., 1991, "Prediction of Wave-Soldered Fillet Geometry in SMT Applications," ASME Winter Annual Meeting, Dec 1-6,1991, Atlanta GA.
Majumdar, S. and Jones, W. B., 1991, "How Well Can We Predict the Lifetime of a Well-Characterized Material", Solder Mechanics: A State of the Art Assessment, D. R. Frear, W. B. Jones and K. R. Kinsman, eds., TMS publications, Warrendale, PA.
Manson, S. S., 1953, "Behavior of Materials Under Conditions of Thermal Stress", Heat Transfer Symposium, Univ. of Michigan, June 27-28,1952, Univ. of Mich. Press; also NACA TN2933.
Manson, S. S., 1960, Mech. Des. V32(14), pp. 139-144.
Pan, T.-Y., Winterbottom, W. L., 1990, "Thermal Cycling Induced Plastic Deformation in Solder Joints", ASME Winter Annual Meeting, Dallas, TX.
Pao, Y. H., Pan, T. Y., 1990, Trans. ASME, J. Electron. Pack., Trans., vol. 112, pp. 154-161.
Pao, Y.-H., Govila, R., Badgley, S., Jih, E., 1993, "An Experimental and Finite Element Study of Thermal Fatigue Fracture of PbSn Solder Joints", J. Electron. Packaging, vol. 115, pp. 1-8.
Rohde, R. W., and J. C. Swearengen, "Deformation modeling applied to stress relaxation of four solder alloys," J. Eng. Mat. Tech., 102, pp. 207-214, 1980.
Ross, R. G., Wen, L. C., Mon, G. R., Jetter, E., 1992, "Solder Creep-Fatigue Interactions with Flexible Leaded Parts", J. Electron. Packaging, vol. 114, pp. 185-192.
Sandor, B. I., 1991, "Lifetime Prediction of Solder Joints: Engineering Mechanics Methods", in Solder Mechanics: A State of the Art Assessment, D. R. Frear, W. B. Jones, K. R. Kinsman, eds., TMS Publications, Warrendale, PA.
Sandstrom, R., Osterberg, J.-O., Nylen, M., 1993, "Deformation Behavior During Low Cycle Fatigue Testing of 60Sn-40Pb Solder", Materials Science and Technol., vol. 9, pp. 811-819.
Sauber, J., Seyyedi, 1992, "Predicting Thermal Fatigue Lifetimes for SMT Solder Joints", J. Electron. Packaging, vol. 114, pp. 472-476.
Schmidt, C. G., 1992, "A Simple Model for Fatigue of Leadless Ceramic Chip Carrier Solder Attachments", J. Electronics Manufac., vol. 2, pp. 31-36.
Solomon, H. D., 1994, "Life Prediction and Accelerated Testing", in The Mechanics of Solder Alloy Interconnects, D. R. Frear, H. S. Morgan, S. N. Burchett, J. Lau, eds., Van Nostrand Reinhold, New York, NY.
Solomon, H. D., Brozowski, V., Thompson, D. G., 1990, Proc. 40th Electron. Comp. and Tech, Conf., Las Vegas, NV, pp. 351-359.
Stone, D. S., and M. M. Rashid, "Constitutive models," in "The Mechanics of Solder Alloy Interconnects", D. R. Frear, S. N. Burchett, H. S. Morgan, and J. H. Lau, eds., pp. 87-157, Van Nostrand Reinhold, 1994.
Verma, S., Dasgupta, A., Barker, D., 1993, "A Numerical Study of Fatigue Life of J-Leaded Solder Joints Using the Energy Partitioning Approach", J. Electron. Packaging, vol. 115, pp. 416-423.
Wong, B, Helling, D. E., Clark, R. W., 1988, IEEE Trans, CHMT, vol. 11, pp. 284-290.
Yamada, S. E., 1987, Eng. Fract. Mech, vol. 27, pp. 315-328.
Yamada, S. E., 1988, Eng. Fract. Mech, vol. 29, pp. 673-682.

Distribution:

MS0841 9100 P.J. Hommert
MS0828 9102 R.D. Skocypec (Route to 9111)
MS0443 9117 H.S. Morgan (Route to Staff)
MS0437 9118 R.K. Thomas
MS0443 9117 QA File
MS0443 9117 S.N. Burchett (10)
MS0443 9117 M.K. Neilsen
MS1435 1800 H.J. Saxton
MS1407 1811 Clough, R.L.
MS1407 1811 D.R. Frear (10)
MS9018 8940-2 Central Technical Files
MS0899 4414 Technical Library (5)
MS0619 12690 Review & Approval, for DOE/OSTI (2)